EUROPEAN ORGANIZATION FOR NUCLEAR RESEARCH

CERN/EP 81-121
30 September 1981

NEUTRAL STRANGE PARTICLE PRODUCTION IN PROTON-PROTON COLLISIONS AT $\sqrt{s}$ = 63 GeV

CERN-Dortmund-Heidelberg-Warsaw Collaboration

D. Drijard, H.G. Fischer, H. Frehse, P. Hanke, P.G. Innocenti, J.W. Lamsa(*), W.T. Meyer(*), G. Mornacchi, A. Norton, O. Ullaland and H. Wahl(**)
CERN, European Organization for Nuclear Research, Geneva, Switzerland

W. Hofmann, T. Lohse, M. Panter, K. Rauschnabel, J. Spengler and D. Wegener
Institut für Physik der Universität Dortmund, Germany

W. Geist, M. Heiden, W. Herr, E.E. Kluge, T. Nakada, A. Putzer and B. Rensch
Institut für Hochenergiephysik der Universität Heidelberg, Germany

K. Doroba, R. Gokieli and R. Sosnowski
University and Institute for Nuclear Research, Warsaw, Poland

ABSTRACT

The inclusive cross section for the production of K^o_s mesons, Λ and $\bar{\Lambda}$ particles in proton-proton interactions at $\sqrt{s}$ = 63 GeV is presented. The produced particles have been detected in the full phase space. Behaviour of the longitudinal and transversal dependences of the cross sections are discussed. The total production cross sections for K^o_s mesons and Λ particles was determined to $\sigma_{K^o_s} = (25.5 \pm 1.4)$mb and $\sigma_\Lambda = (7.8 \pm 1.2)$mb respectively. A strong energy dependence of the production cross sections is observed.

Submitted to Zeitschrift für Physik C

(*) Visitor from Ames Laboratory, Iowa State University, USA.
(**) Now at Institut für Hochenergiephysik, Vienna, Austria.

EP/0418P/DW/ef

1. INTRODUCTION

The investigation of strange particle production in hadronic interactions at high energies is of particular interest, since a new quantum number is created. Hence, the dynamical behaviour of these reactions could resemble the hadronic production of charmed particles. The latter process shows two unexpected features, namely a high production cross section and a weak dependence of the inclusive cross section on the longitudinal momentum [1]. A detailed investigation of strange particle production might help to disentangle the sources responsible for this unusual behaviour of charmed particle production.

Up to now detailed measurements for the reactions

$$pp \to K^0_s + X \tag{1a}$$

$$pp \to \Lambda + X \tag{1b}$$

$$pp \to \bar{\Lambda} + X \tag{1c}$$

only exist at lower energies [2-14], where phase space effects are of dominating influence and may hide the dynamics of the process. In the region of energies accessible at the CERN proton-proton Intersecting Storage Rings (ISR), the inclusive cross section for neutral strange particle production ($V^0 = K^0_s$, Λ, $\bar{\Lambda}$) production is determined up to now only for limited parts of the phase space [15-17]. The present paper describes the results of an experiment in which the inclusive cross section for V^0 particle production has been measured in the full phase space (4π steradian) at $\sqrt{s}$ = 63 GeV. The paper is organized as follows: the experimental procedure and the data reduction are described in sect. 2. In sect. 3 the cross sections are presented, whose main features are discussed in sect. 4. In sect. 5 the results are summarized.

2. EXPERIMENT AND DATA REDUCTION

2.1 Experimental set-up and trigger

The experiment was performed at the CERN ISR using the upgraded Split Field Magnet detector (SFM) [18], which allows to measure the momenta of charged particles in 4π steradian. In previous publications, the

experimental set-up [18-19] and the trigger (minimum bias trigger), have been described [20,21]. The cross section seen by the trigger amounts to $\sim$ 95% of the inelastic cross section. The results discussed in this paper are based on a total number of 58 200 triggers corresponding to 120 ms open time of the detector.

The raw data were processed with the SFM off-line program chain to reconstruct those tracks which result from the primary interaction vertex. The overall efficiency for detecting a particle and reconstructing its track in the detector is larger than 75% for positive and 84% for negative tracks. It has been checked that the efficiency of the program is independent of the charged multiplicity of the event.

2.2 V^0 particle reconstruction

In a second stage of the analysis, the secondary vertices from V^0 decays were reconstructed. A special fit procedure was designed to determine simultaneously the geometrical and kinematical variables of a V^0 decay, taking into account the relations between these variables due to the magnetic field. A detailed description of this procedure is given in ref. [22]. In fig. 1(a-c) the distributions of the invariant mass after the vertex fit is shown for those V^0 particles, where the momentum is determined with a precision of $\Delta p/p < 0.1$ and where the decay length ℓ is five times larger than the error on its decay length, determined in the fit. The mass resolution is 40 MeV FWHM and 10 MeV FWHM for K^0_s mesons and Λ particles respectively.

The acceptances for V^0 reconstruction at different stages of the analysis are shown in figs 2(a,b) as functions of the rapidity y in the proton-proton c.m. system:

(a) after track finding where both tracks are found,

(b) after the V^0 fit.

Different kinds of losses can be observed: for small y (low momenta) losses are mainly due to track finding efficiency (it is in particular rather low for the pion from a $\Lambda/\bar{\Lambda}$ decay) and to the cuts imposed on the decay length. For larger momentum, some V^0's are lost because of the

small opening angle, giving rise to large errors on the secondary vertex position. Further losses at large rapidities are explained by the small production angle. These tracks cross a relatively large amount of material, if the V^0 decays inside the beam tube. Furthermore, any scattering in the beam tube is amplified by the long lever arm between the beam tube exit and the first observation of the track and therefore causes rather large deviations between the observed and expected position of the first measurement.

It should be noted that the acceptance depends in addition on the azimuthal angle ϕ. It has been checked that the number of observed V^0 does not depend on ϕ after acceptance corrections have been applied.

In fig. 3(a) the lifetime distribution for K^o_s mesons is shown. The straight line corresponds to the world average [23]. At short decay length $c\tau \lesssim 1$ cm losses are observed. The corresponding distributions for Λ and $\bar{\Lambda}$ particles are shown in fig. 3(b-c). Also in this case the agreement between the lifetime as measured in this experiment and table values [23] is satisfactory.

As usual, the fit results not in all cases in a unique mass assignment. This is demonstrated by fig. 4, which shows the decay angular distribution for K^o_s mesons, where θ^* is the angle between the the momenta of the π^+ and of the K^o_s meson in the K^o_s rest system. Results are shown for unique and all K^o_s meson solutions, where the latter also includes the K^o_s/Λ and $K^o_s/\bar{\Lambda}$ ambiguities respectively. The K^o_s-all distribution is significantly disturbed by Λ and $\bar{\Lambda}$ particle contamination. This is more clearly demonstrated in fig. 5, where the K^o_s meson contribution has been determined by a Monte-Carlo calculation, which is normalized to the K^o_s-unique solution in the range $|\cos\theta^*| < 0.6$. As is well known [24], the forward peak ($\cos\theta^* \sim 1$) and the backward peak ($\cos\theta^* \sim -1$) are due to leaks from respectively Λ and $\bar{\Lambda}$ particles kinematically compatible with K^o_s assignment. Since the probabilities for K^o_s/Λ and $K^o_s/\bar{\Lambda}$ confusion are evidently equal, the relative importance of these leakages give already some information on the $\Lambda/\bar{\Lambda}$ production cross section.

The decay angular distributions for Λ and $\bar{\Lambda}$ particles are plotted in figs 6 and 7 respectively. The plots exhibit two pecularities: first the distributions are asymmetric, especially that for Λ particles. It has a dip at $\cos\theta^* \sim 0.2$, where most Λ particles are ambiguous with a K^o_s meson. This feature is reproduced quantitatively by Monte-Carlo studies [22]. In addition, a narrow spike exists at $|\cos\theta^*| = 1$, which is due to e^+e^- pairs resulting from γ conversion. Its contribution is removed by the cut $\cos\theta^* < -0.98$ for Λ and $\cos\theta^* > +0.98$ for $\bar{\Lambda}$ particles respectively, which corresponds to a transverse momentum of $p_T < 20$ MeV/c relative to the $\Lambda(\bar{\Lambda})$ direction.

The study of the sources of background, losses and ambiguities has led us to apply the following cuts to obtain a sample of uniquely reconstructed V^0 particles:

- V^0 fit with $\chi^2 < 18$,
- momentum uncertainty $\Delta p/p < 0.1$,
- decay length $\ell \geq 1$ cm,
- $\ell \geq 5 *$ uncertainty of decay length,
- $\cos\theta^*$ cut to remove e^+e^- pairs in $\Lambda(\bar{\Lambda})$ sample.
- $p_{lab} \geq 0.1$ GeV/c.

After these cuts the probability to misidentify V^0 particles is smaller than 5%.

3. EXPERIMENTAL RESULTS

A sample of 58 200 minimum bias events was used to determine the differential and total cross section for the reactions (1). The sample of uniquely reconstructed V^0 particles analyzed in this experiment, consists of 2773 K^o_s mesons, 758 Λ particles and 471 $\bar{\Lambda}$ particles. Only data in phase space regions, where the acceptance is larger than 5% have been used for cross section calculations. This acceptance includes the condition of the unambiguous identification of a V^0. The data have been corrected for detector acceptances including the cuts discussed in sect. 2.2, reconstruction efficiency and the branching ratios for the observed channels $K^o_s \to \pi^+\pi^-$,

$\Lambda \to p\pi^-$ and $\bar{\Lambda} \to \bar{p}\pi^+$. The absolute normalization was done with the help of luminosity monitor counters calibrated by the van der Meer method [25]. The error is of the order of 4%. The error bars given in the figures correspond to the statistical error only.

3.1 Inclusive K^o_s meson production

In fig. 8 the Lorentz invariant cross section is plotted as a function of rapidity y for three intervals of the transverse momentum p_T. A rapidity plateau of ± 2 units is observed.

The transverse momentum distribution is shown in fig. 9; it is compatible with an exponential dependence on p_T.

$$E \frac{d^3\sigma}{dp^3} \sim e^{-bp_T}$$

A fit to our data gives a slope of $b = (4.68 \pm 0.08)(GeV/c)^{-1}$. This value is compatible with the values found for the production of K^+ and K^- mesons [26,27]. The p_T dependence of the Lorentz invariant cross section at y = 0 is shown in fig. 10; for comparison the results of Büsser et al. [15] at lower ISR energies (averaged over the energy interval 30 GeV < $\sqrt{s}$ < 53 GeV) are included. The mean value

$$E \frac{d^3\sigma}{dp^3} = \frac{1}{2} \left\{ E \frac{d^3\sigma}{dp^3} (pp \to K^+ + X) + E \frac{d^3\sigma}{dp^3} (pp \to K^- + X) \right\} \qquad (2)$$

of ref. [27], calculated from the fit to their data, is in good agreement with the cross section of reaction (1a) as measured in this experiment (solid lines in fig. 8).

The total cross section for the reaction (1a) has been determined from the present data under the assumption that the Lorentz invariant cross section factorizes in rapidity and transverse momentum

$$E \frac{d^3\sigma}{dp^3} = \frac{d\sigma}{dy} e^{-bp_T} \quad . \qquad (3)$$

Extrapolating the measured values to p_T = 0 GeV/c and summing over all rapidities one gets a total inclusive cross section of $\sigma(pp \to K^o_s + X)$ = (25.5 ± 1.4)mb, which is plotted together with the results at lower energies in fig. 11. The uncertainty of the normalization and the p_T

extrapolation is included in the error. A steep increase of the production cross section in the energy region covered by the ISR is observed. The results of ref. [27] indicate a similar behaviour of charged K-mesons.

3.2 Lambda particle production

The Lorentz invariant cross section for the reaction (1b) is plotted as a function of the Feynman variable x in fig. 12 for three intervals of the transverse momentum. For comparison, the results of ref. [16] in the fragmentation region are included (full line). The two experiments are in good agreement.

In fig. 13 the transverse momentum distribution for Λ particle production is shown. The shape of the distribution is similar to that one for proton production [26]

$$E \frac{d^3\sigma}{dp^3} \sim e^{-4p_T} , \qquad (4)$$

which is included in the figure (full line). A fit to our data results in a slope of $b = (4.02 \pm 0.12)(GeV/c)^{-1}$. The p_T dependence of the Lorentz invariant cross section at $x = 0$ as determined in the present experiment, is compared with the results of ref. [15] in fig. 14. The results are in agreement, if one allows for an increase of the production cross section with energy.

Assuming again that factorization holds (formula (3)), the total inclusive cross section for Λ production has been derived from the measured differential cross section. The value obtained is $\sigma(pp \to \Lambda + X) = (7.8 \pm 1.2)mb$. It is shown together with the results of other experiments in fig. 15. The inclusive cross section for Λ production increases in the energy region of the ISR. The results of this experiment are compatible with those of ref. [16], where lower limits of the total cross section for reaction (1b) were derived.

3.3 Antilambda particle production

The transverse momentum dependence of the inclusive cross section for $\bar{\Lambda}$ production is shown in fig. 16; the observed shape is compatible with that for $\bar{p}$ production [27] in proton-proton collisions. The p_T dependence of the Lorentz invariant cross section at $x = 0$ is compared separately

in fig. 17 with the results of ref. [15] obtained at lower ISR energies. The results of the present experiment are appreciable larger than those of ref. [15] measured at lower energies, which indicates an increase of the production cross section for reaction (1c) in the energy region of the ISR.

4. DISCUSSION OF THE RESULTS

The production cross section for K^o_s mesons in proton-proton collisions shows the same rapidity and transverse momentum dependence as the cross section for K^+/K^- production (figs 8 and 10). This behaviour is expected in constituent models of particle production [28], since the quark content of the detected K^o_s mesons is comparable to the quark composition of a mixture of charged K mesons. The observed increase of the inclusive cross section (fig. 11) with energy is compatible with a dominant central production mechanism [17].

The observed longitudinal behaviour of the inclusive cross section for K^o_s mesons differs from that for D^+ meson production [1]. This difference may be due to the different masses of the particles.

The Λ production shows a similar behaviour as the production of neutrons and protons, if the diffractive component of the latter is removed. The similarity is demonstrated by fig. 18, where the x dependence of the Lorentz invariant cross section for the reaction [29]

$$pp \rightarrow n + X$$

and the result of the present experiment for the reaction (1b) are compared. The cross sections have the same shape. The Λ production is suppressed as compared to the neutron production by a factor which is compatible with the observations in other strange particle production reactions [17,28,30].

The x and p_T dependence of the $\bar{\Lambda}$ production displays a similar behaviour as $\bar{p}$ production in proton-proton interactions, especially if one compares it with the dependence observed for their respective antiparticles. $\bar{\Lambda}$ production therefore seems to be due to a central process as $\bar{p}$ production.

The most prominent effect observed for all three production cross sections is its strong increase with energy, which is e.g. for K^o_s mesons appreciably steeper than that for π mesons [27]. This observation indicates that even at the highest ISR energy an asymptotic behaviour for the production of heavy flavours has not been reached.

5. CONCLUSIONS

In this paper the inclusive cross section for the production of K^o_s mesons, Λ and $\bar{\Lambda}$ particles, measured at the highest presently accessible energies, have been presented. The data have been recorded in the full phase space. We reach at the following conclusions:

(i) The K^o_s meson production is compatible to the mean value of the K^+ and K^- meson productions. In the energy interval covered by the ISR the total cross sections for K^o_s meson production increases by a factor of 3, while the corresponding increase of π mesons amounts only to a factor of 1.6.

(ii) The inclusive cross section for Λ particle production is similar to that one for neutrons $\sigma(pp \to \Lambda + X)$; it increases strongly with energy.

(iii) $\bar{\Lambda}$ production shows a similar transverse momentum behaviour as $\bar{p}$ production. The Lorentz invariant cross section at $y = 0$ increases strongly with energy.

The observed features are in concordance with the expectations of constituent models for particle production.

Acknowledgement

This experiment was greatly helped by contributions from the SFM detector group. We are indebted to the ISR Experimental Support group. We acknowledge the important help from R. Messerli. The Dortmund and the Heidelberg groups were supported by a grant from the Bundesministerium für Wissenschaft und Forschung of the Federal Republic of Germany.

REFERENCES

[1] ACCDHW Collaboration, D. Drijard et al., Phys. Lett. 81B (1979) 250;
D. Drijard et al., Phys. Lett. 85B (1979) 452.

[2] K. Jaeger et al., Phys. Rev. D11 (1975) 1756.

[3] V. Blobel et al., Nucl. Phys. B69 (1974) 454;
H. Fesefeldt et al., Nucl. Phys. B135 (1978) 379.

[4] H. Bøggild et al., Nucl. Phys. B57 (1973) 77;
P. Achlin et al., Physica Scripta 21 (1980) 12.

[5] H. Blumenfeld et al., Phys. Lett. 45B (1973) 528.

[6] M. Alston-Garnjost, Phys. Rev. Lett. 35 (1975) 142.

[7] J.W. Chapman et al., Phys. Lett. 47B (1973) 465.

[8] D. Brick et al., Nucl. Phys. B164 (1980) 1.

[9] K. Jaeger et al., Phys. Rev. D11 (1975) 2405.

[10] A. Sheng et al., Phys. Rev. D11 (1975) 1733.

[11] F.T. Dao et al., Phys. Rev. Lett. 30 (1973) 1151.

[12] F. LoPinto et al., Phys. Rev. D22 (1980) 573.

[13] R.D. Kass et al., Phys. Rev. D20 (1979) 605.

[14] H. Kichimi et al., Phys. Rev. D20 (1979) 37.

[15] F.W. Büsser et al., Phys. Lett. 61B (1976) 309.

[16] S. Erhan et al., Phys. Lett. 85B (1979) 447.

[17] ACCDHW Collaboration, D. Drijard et al., Zeitschr. für Physik C 9 (1981) 293.

[18] W. Bell et al., Nucl. Instr. & Meth. 156 (1978) 111.

[19] CCHK Collaboration, M. Della Negra et al., Nucl. Phys. B127 (1977) 1.

[20] W. Bell et al., Nucl. Instr. & Meth. 124 (1975) 437.

[21] CCHK Collaboration, D. Drijard et al., Nucl. Phys. B155 (1979) 269.

[22] K. Rauschnabel, V^0 reconstruction in the Split Field Magnet Spectrometer, CERN/EP/Int. Report 81-1, April 1981;
K. Rauschnabel, Thesis University of Dortmund 1981 (unpublished).

[23] Particle Data Group, Rev. Mod. Phys. 52 (1980) S1.

REFERENCES (Cont'd)

[24] J. Podolanski and R. Armenteros, Phil. Mag. 45 (1954) 13.

[25] S. van der Meer, CERN-PO 168-31.

[26] J. Singh et al., Nucl. Phys. B140 (1978) 189.

[27] B. Alper et al., Nucl. Phys. B87 (1975) 19.

[28] V.M. Shekhter and L.M. Skcheklova, Sov. J. Nucl. Phys. 27 (1978) 567.

[29] J. Engler et al., Nucl. Phys. B84 (1975) 70.

[30] L. Van Hove, CERN/TH 2997 (1980);
Yu V. Fisjak and E.P. Kistenev, CERN/EP 80-209.

FIGURE CAPTIONS

Fig. 1 Invariant mass spectrum after the secondary vertex fit for good V^0's [22]: (a) $K^0_s \to \pi^+\pi^-$, (b) $\Lambda \to p\pi^-$ and (c) $\bar{\Lambda} \to \bar{p}\pi^+$.

Fig. 2 Acceptance at different stages of analysis.

Fig. 3 Lifetime distribution after application of acceptance corrections for unique: (a) K^0_s mesons, (b) Λ particles and (c) $\bar{\Lambda}$ particles. The full line corresponds to the table values [23].

Fig. 4 Decay angular distribution for unique and all K^0_s mesons.

Fig. 5 Decay angular distribution of "K^0_s mesons" after subtraction of the K^0_s contribution determined by Monte-Carlo calculations and normalized to the unique K^0_s mesons in the interval $|\cos\theta^*| < 0.6$.

Fig. 6 Decay angular distribution for all and for unique Λ particles.

Fig. 7 Decay angular distribution for all and for unique $\bar{\Lambda}$ particles.

Fig. 8 Lorentz invariant cross section for K^0_s mesons. The full lines represent interpolated values from ref. [27] at $\sqrt{s}$ = 53 GeV.

Fig. 9 Transverse momentum distribution for K^0_s mesons.

Fig. 10 Lorentz invariant cross section at y = 0 as a function of p_T including data from Büsser et al., [15].

Fig. 11 Inclusive cross section for K^0_s meson production as a function of s (o results of ref. [2-17]).

Fig. 12 Lorentz invariant cross section for Λ production including the results of ref. [16] as full lines.

FIGURE CAPTIONS (Cont'd)

Fig. 13 Transverse momentum distribution for Λ particles. The full line represents the shape measured for proton production [27].

Fig. 14 Lorentz invariant cross section as a function of p_T at $y = 0$, data of ref. [15] are included.

Fig. 15 Inclusive cross section for Λ production as a function of s (o results of ref. [2-17]).

Fig. 16 Transverse momentum distribution for $\bar{\Lambda}$ particles. The full line represents the shape measured for $\bar{p}$ production [27].

Fig. 17 Lorentz invariant cross section for $\bar{\Lambda}$ production at $y = 0$ as a function of p_T, data from ref. [15] are included.

Fig. 18 Comparison of the Lorentz invariant cross section at $p_T = 0.4$ GeV for $pp \rightarrow \Lambda + X$ as measured in this experiment and for $pp \rightarrow n + X$ [29].

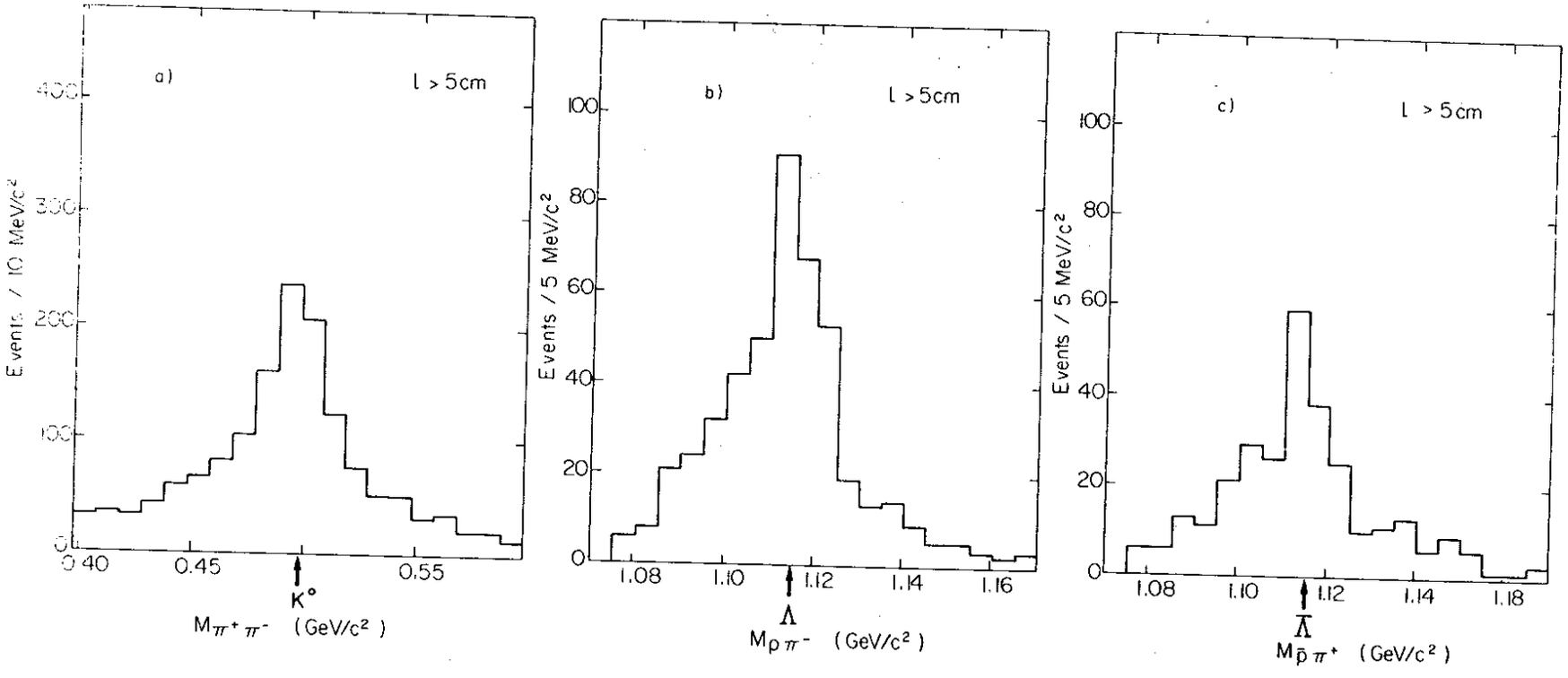
a)
l > 5cm
Events / 10 MeV/c²
0.40
0.45
0.55
K°
Mπ⁺π⁻ (GeV/c²)
b)
l > 5cm
Events / 5 MeV/c²
1.08
1.10
1.12
1.14
1.16
Λ
Mpπ⁻ (GeV/c²)
c)
l > 5cm
Events / 5 MeV/c²
1.08
1.10
1.12
1.14
1.18
Λ̄
Mp̄π⁺ (GeV/c²)

Fig. 1

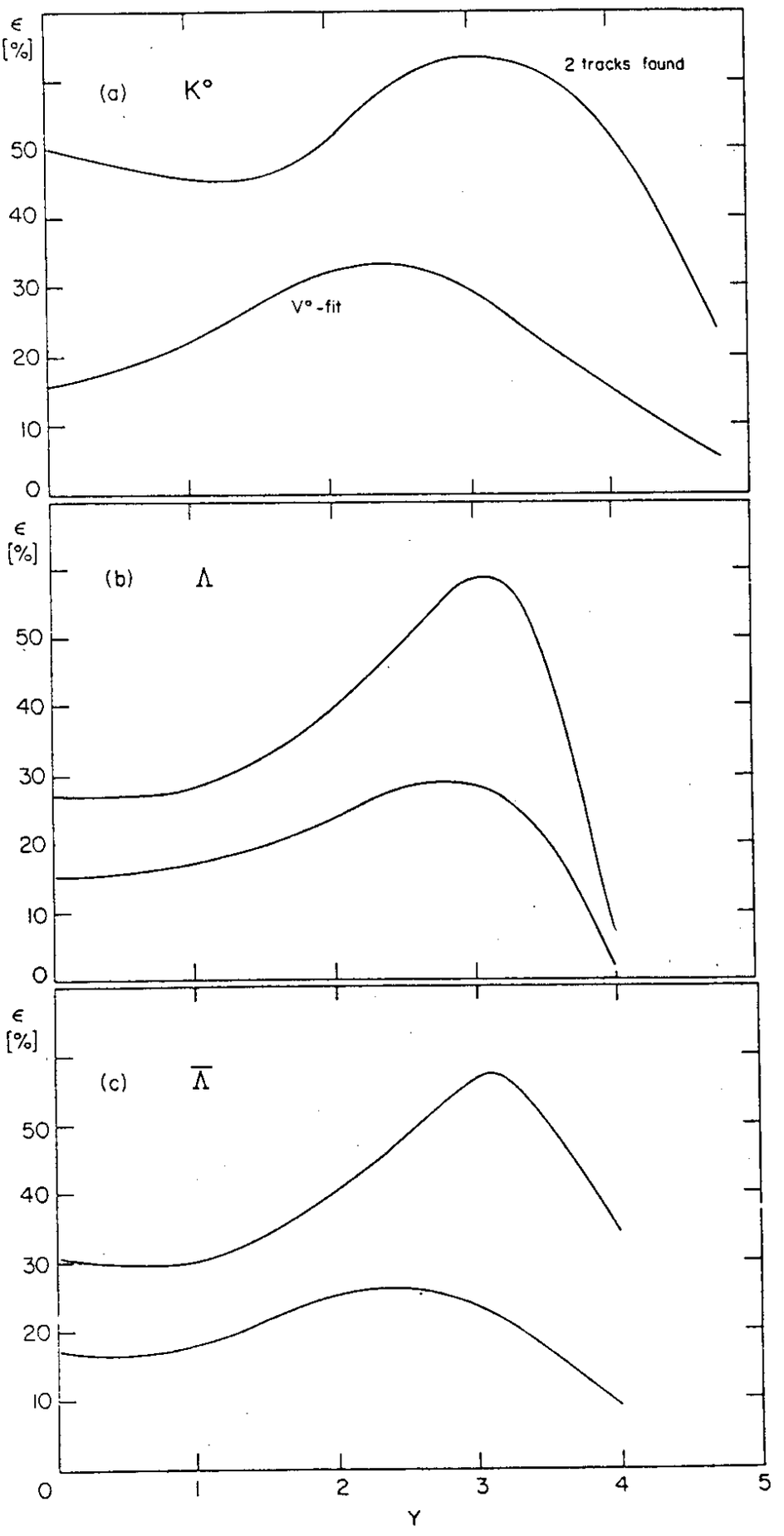
ε [%]
(a) K°
2 tracks found
V°-fit
50
40
30
20
10
0
ε [%]
(b) Λ
50
40
30
20
10
0
ε [%]
(c) $\overline{\Lambda}$
50
40
30
20
10
0
1
2
3
4
5
Y

Fig. 2

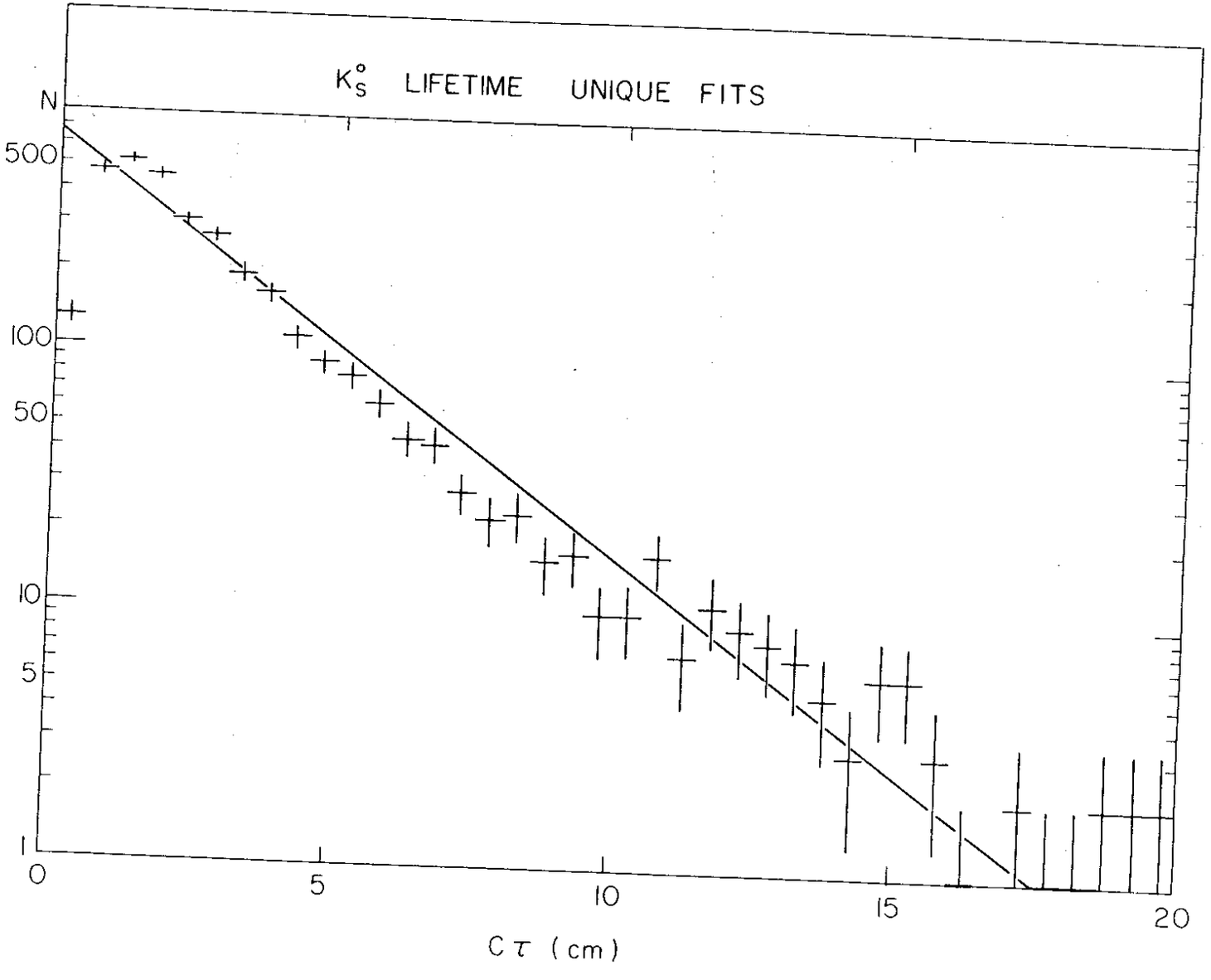
K°_{S} LIFETIME UNIQUE FITS
N
500
100
50
10
5
1
0
5
10
15
20
$C\tau$ (cm)

Fig. 3(a)

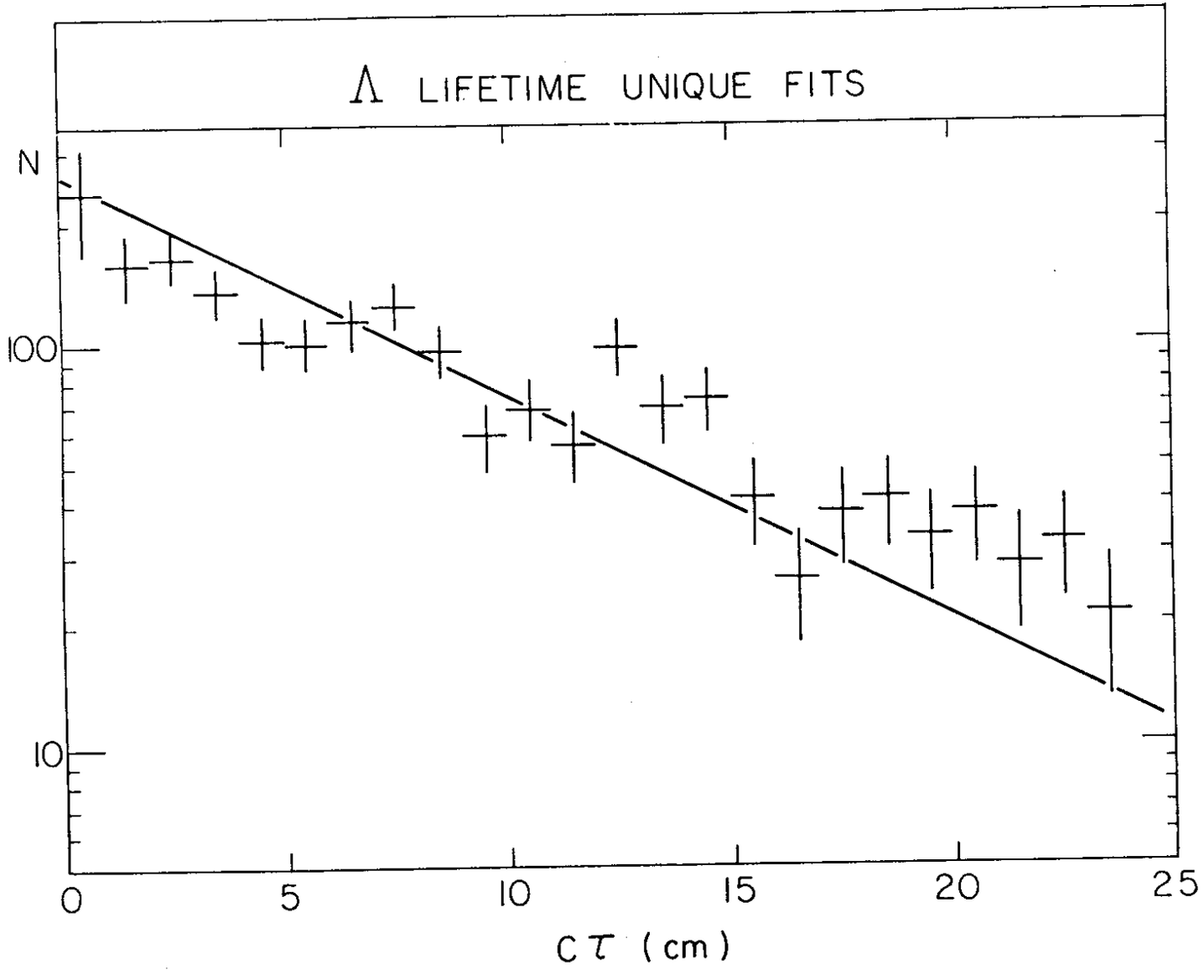

Fig. 3(b)

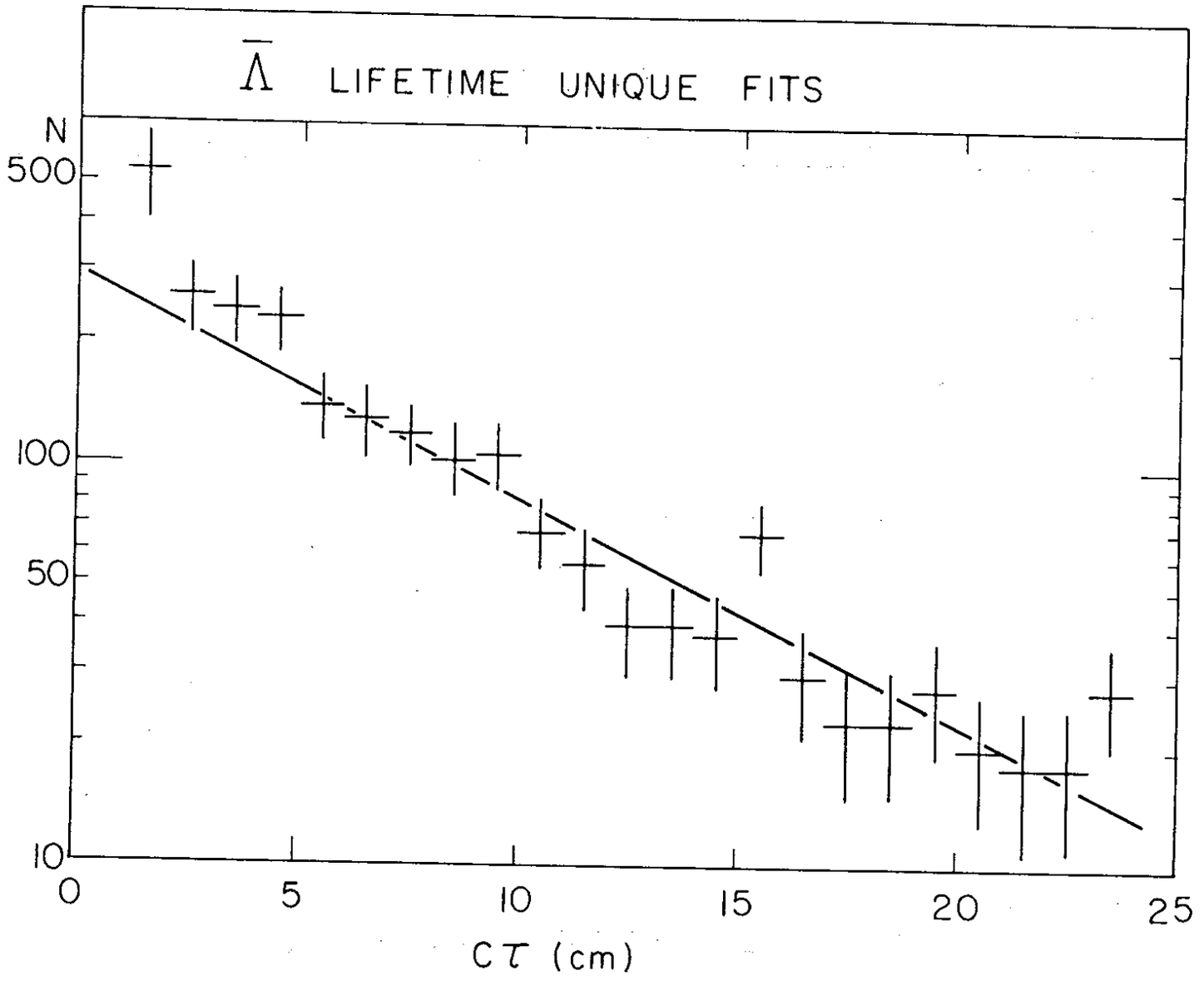
$\bar{\Lambda}$ LIFETIME UNIQUE FITS
N
500
100
50
10
0
5
10
15
20
25
$C\tau$ (cm)

Fig. 3(c)

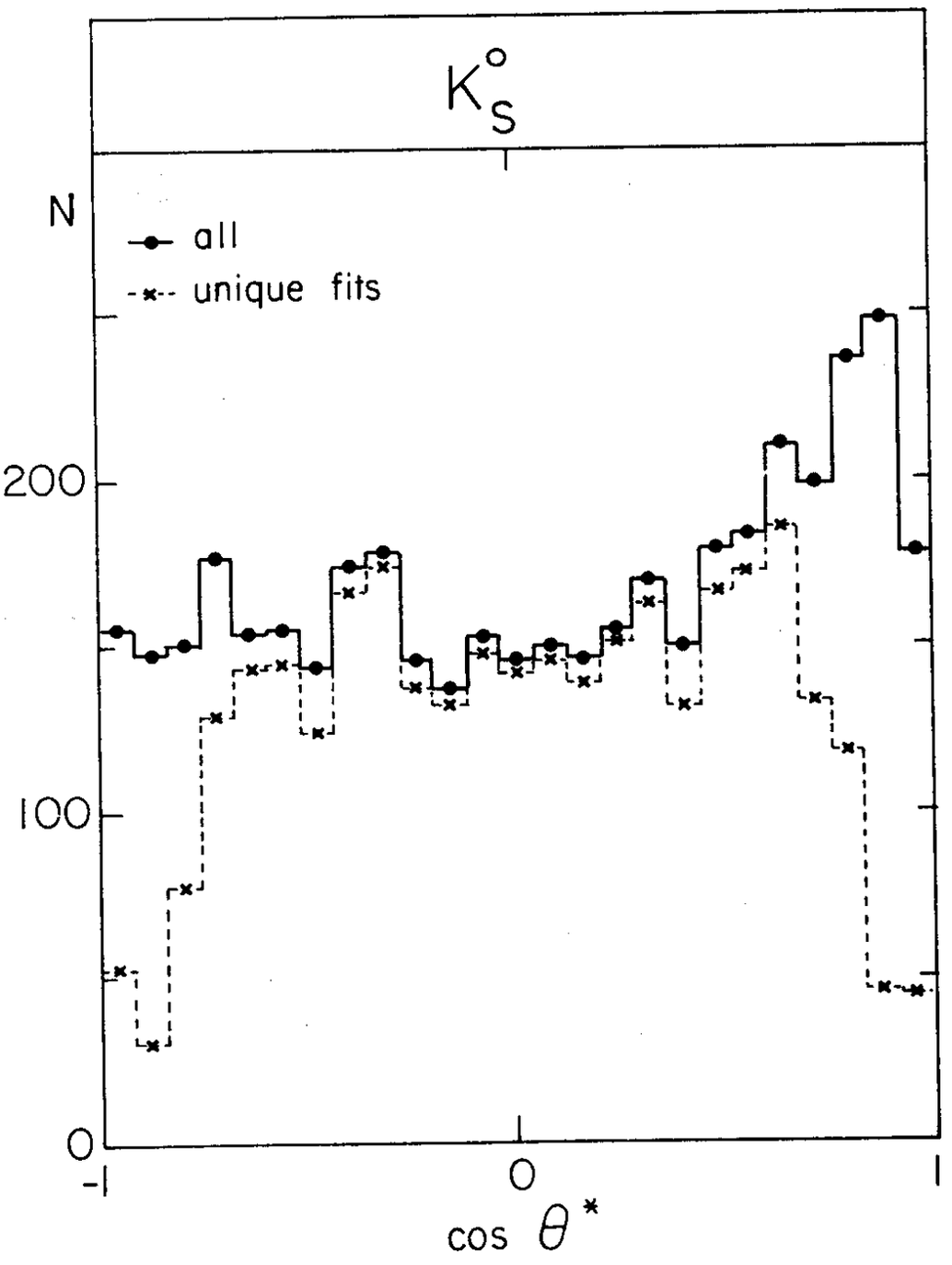

Fig. 4

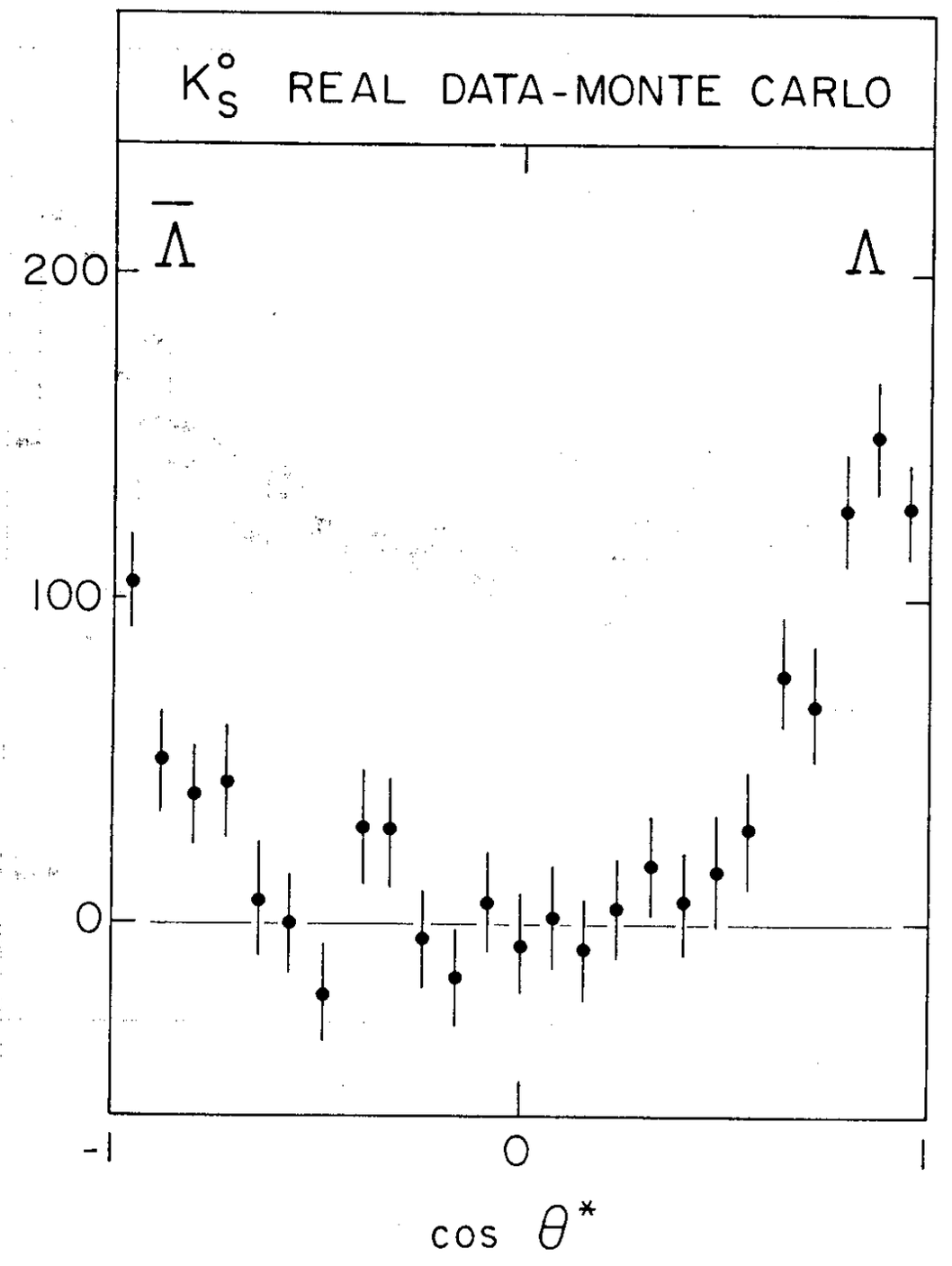
K^0_S REAL DATA-MONTE CARLO
$\bar{\Lambda}$
Λ
200
100
0
-1
0
1
cos θ^*

Fig. 5

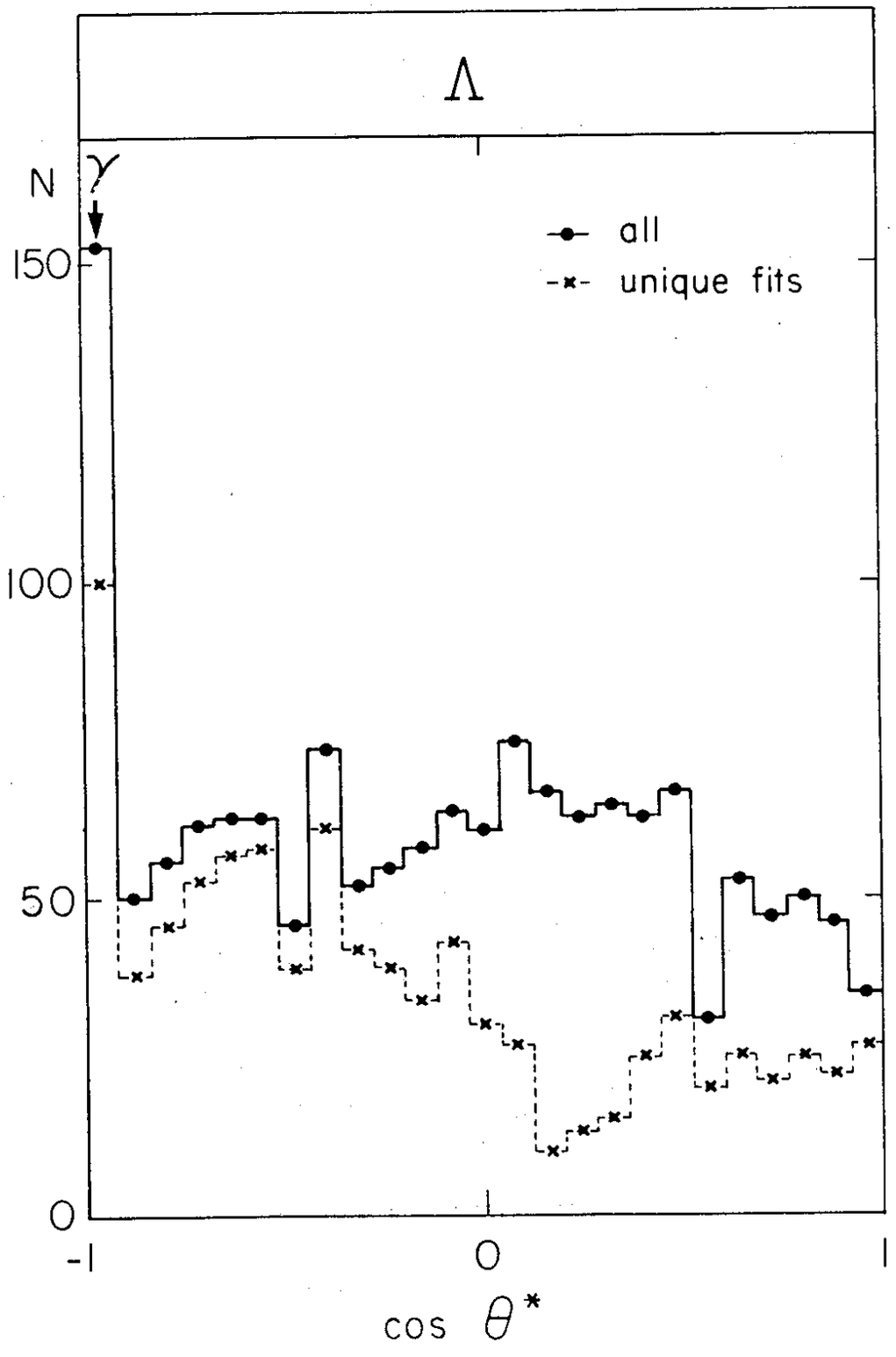

Fig. 6

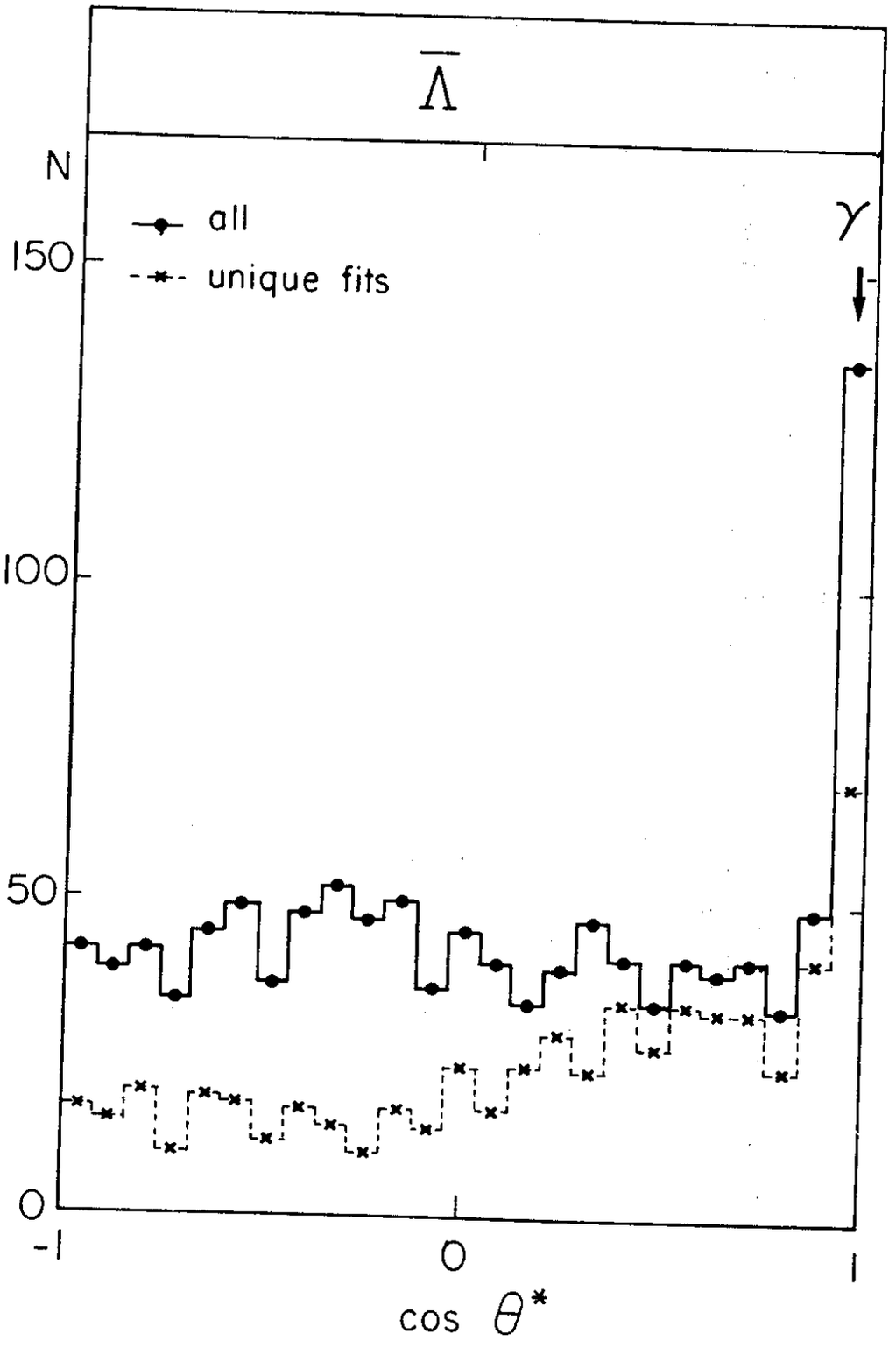

Fig. 7

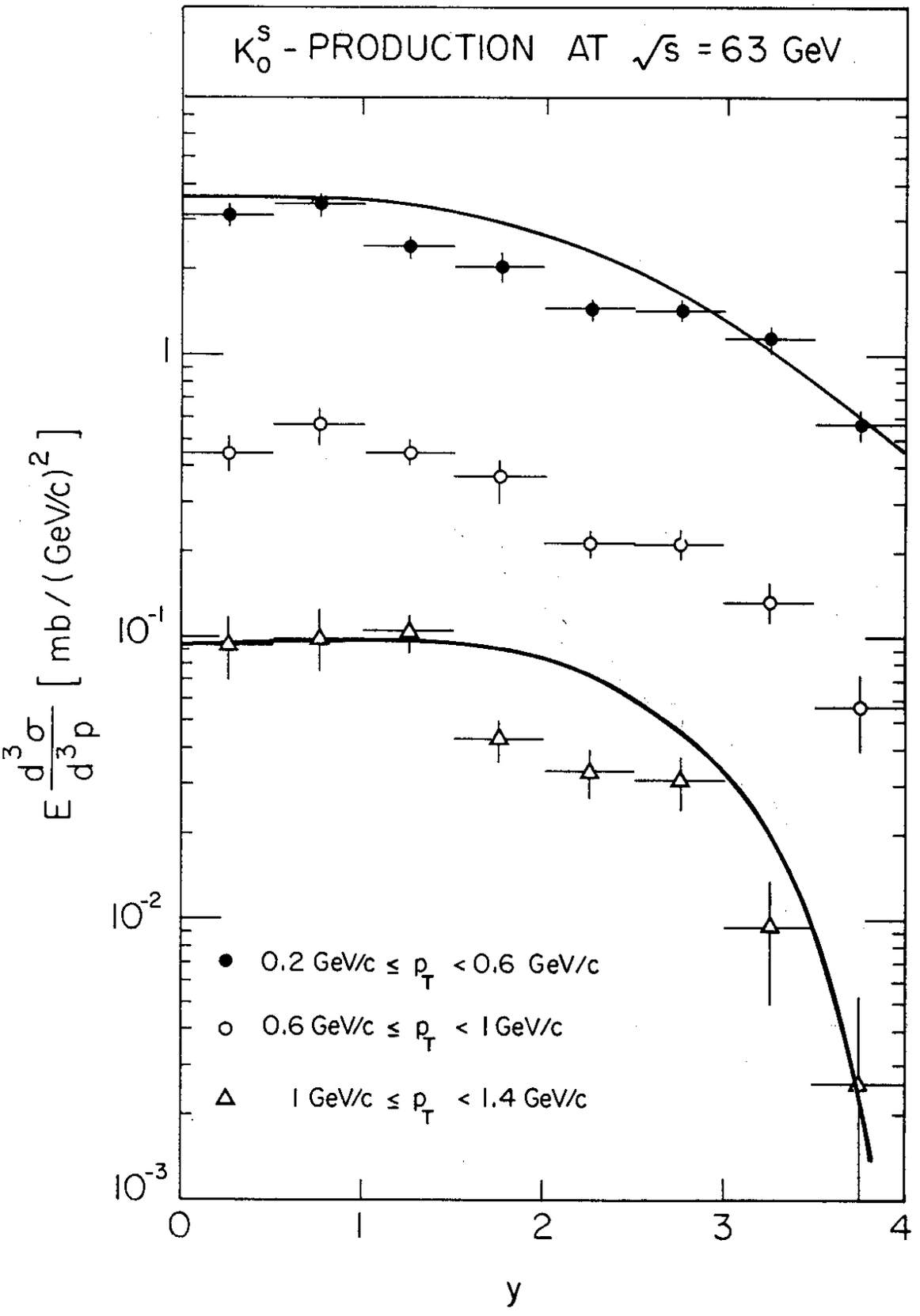
K_0^s - PRODUCTION AT $\sqrt{s}$ = 63 GeV
$E\frac{d^3\sigma}{d^3p}$ [mb / (GeV/c)^2]
1
10^{-1}
10^{-2}
10^{-3}
0
1
2
3
4
y
● 0.2 GeV/c ≤ p_T < 0.6 GeV/c
o 0.6 GeV/c ≤ p_T < 1 GeV/c
△ 1 GeV/c ≤ p_T < 1.4 GeV/c

Fig. 8

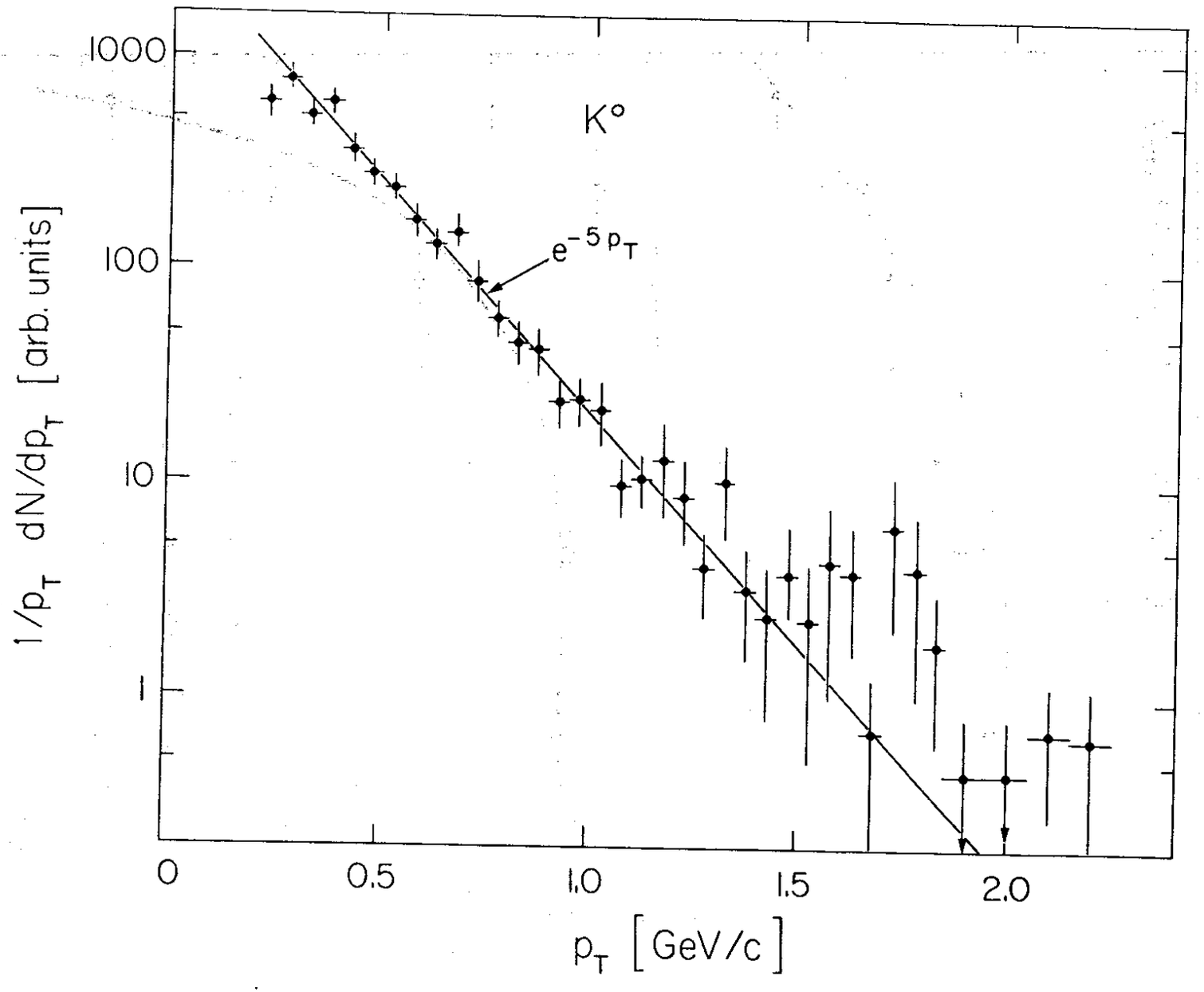

Fig. 9

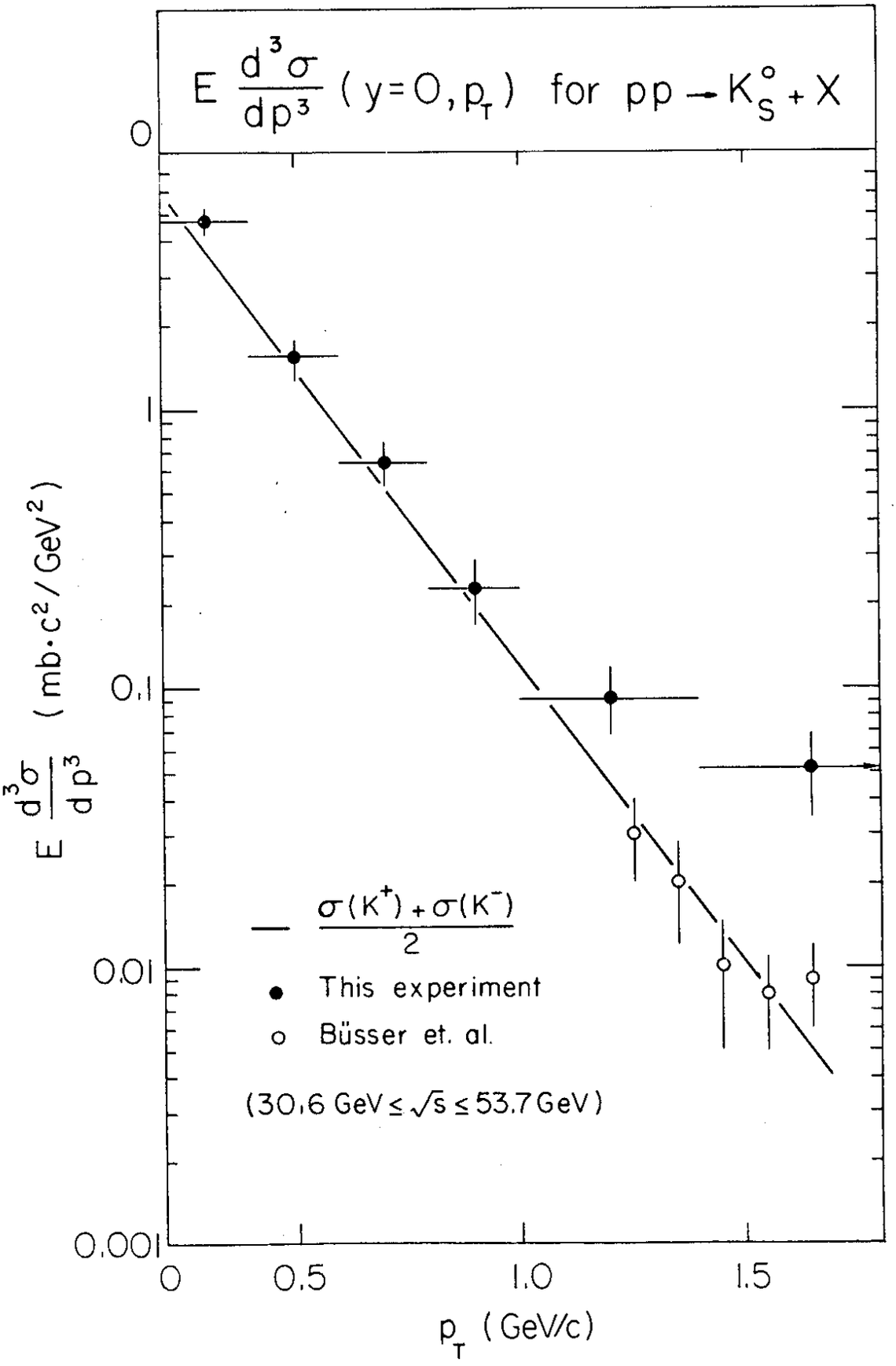
$E\frac{d^3\sigma}{dp^3}(y=0,p_T)$ for $pp \rightarrow K_S^0 + X$
$E\frac{d^3\sigma}{dp^3}$ (mb·c²/GeV²)
$\frac{\sigma(K^+)+\sigma(K^-)}{2}$
This experiment
Büsser et. al.
(30.6 GeV ≤ √s ≤ 53.7 GeV)
p_T (GeV/c)
0
1
0.1
0.01
0.001
0
0.5
1.0
1.5

Fig. 10

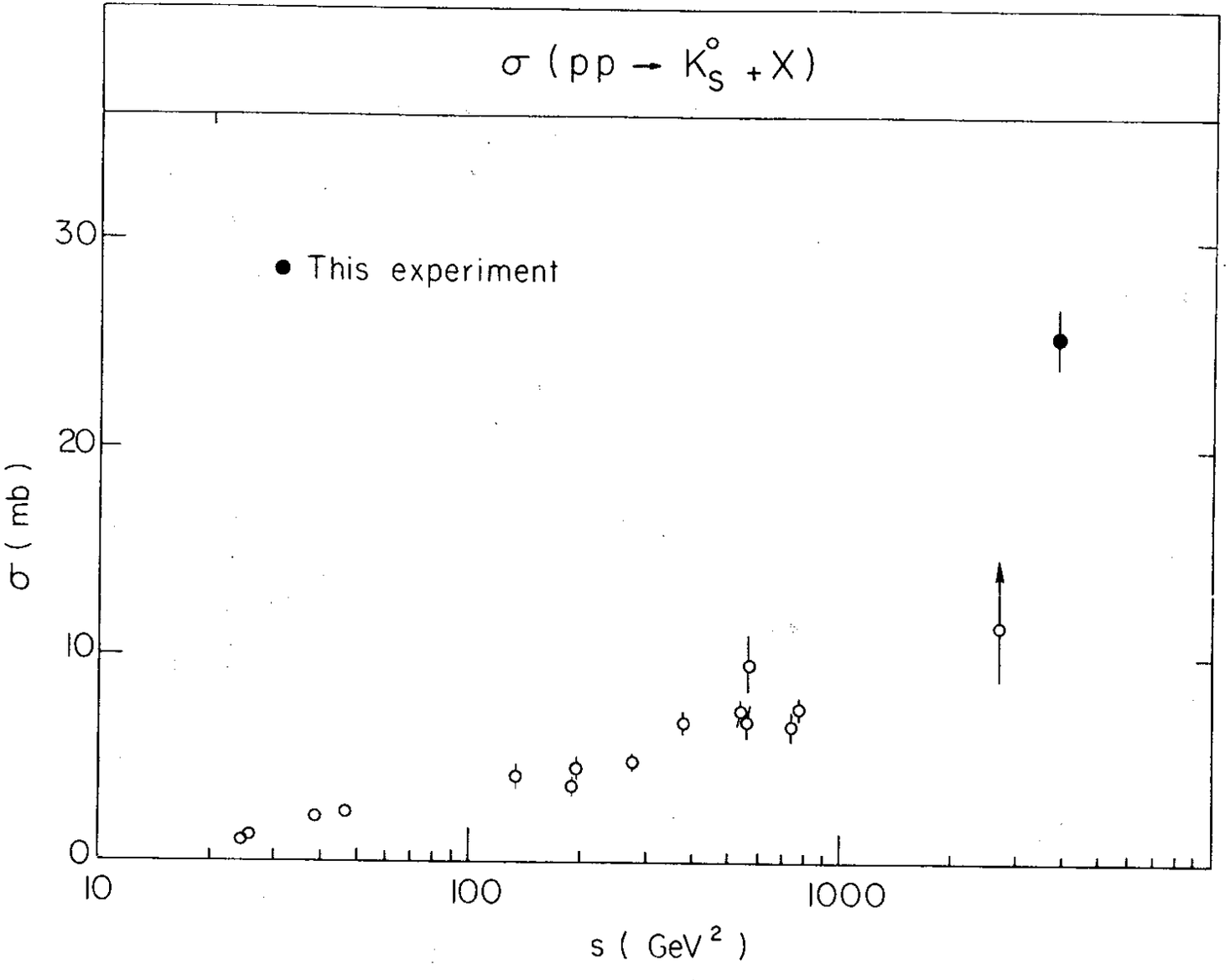

Fig. 11

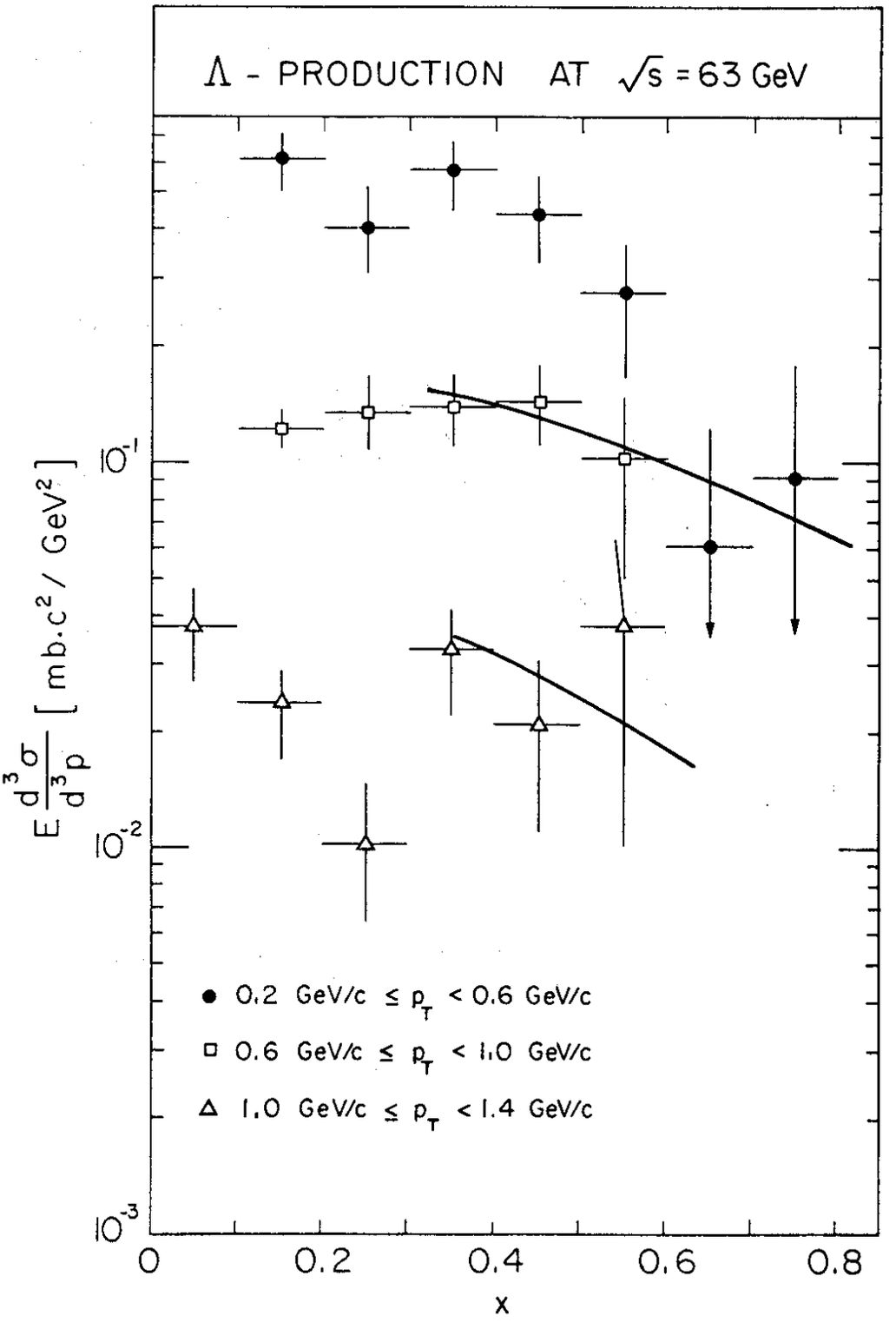
Λ - PRODUCTION AT √s = 63 GeV
E d³σ/d³p [mb.c²/ GeV²]
10⁻¹
10⁻²
10⁻³
0
0.2
0.4
0.6
0.8
x
● 0.2 GeV/c ≤ p_T < 0.6 GeV/c
□ 0.6 GeV/c ≤ p_T < 1.0 GeV/c
△ 1.0 GeV/c ≤ p_T < 1.4 GeV/c

Fig. 12

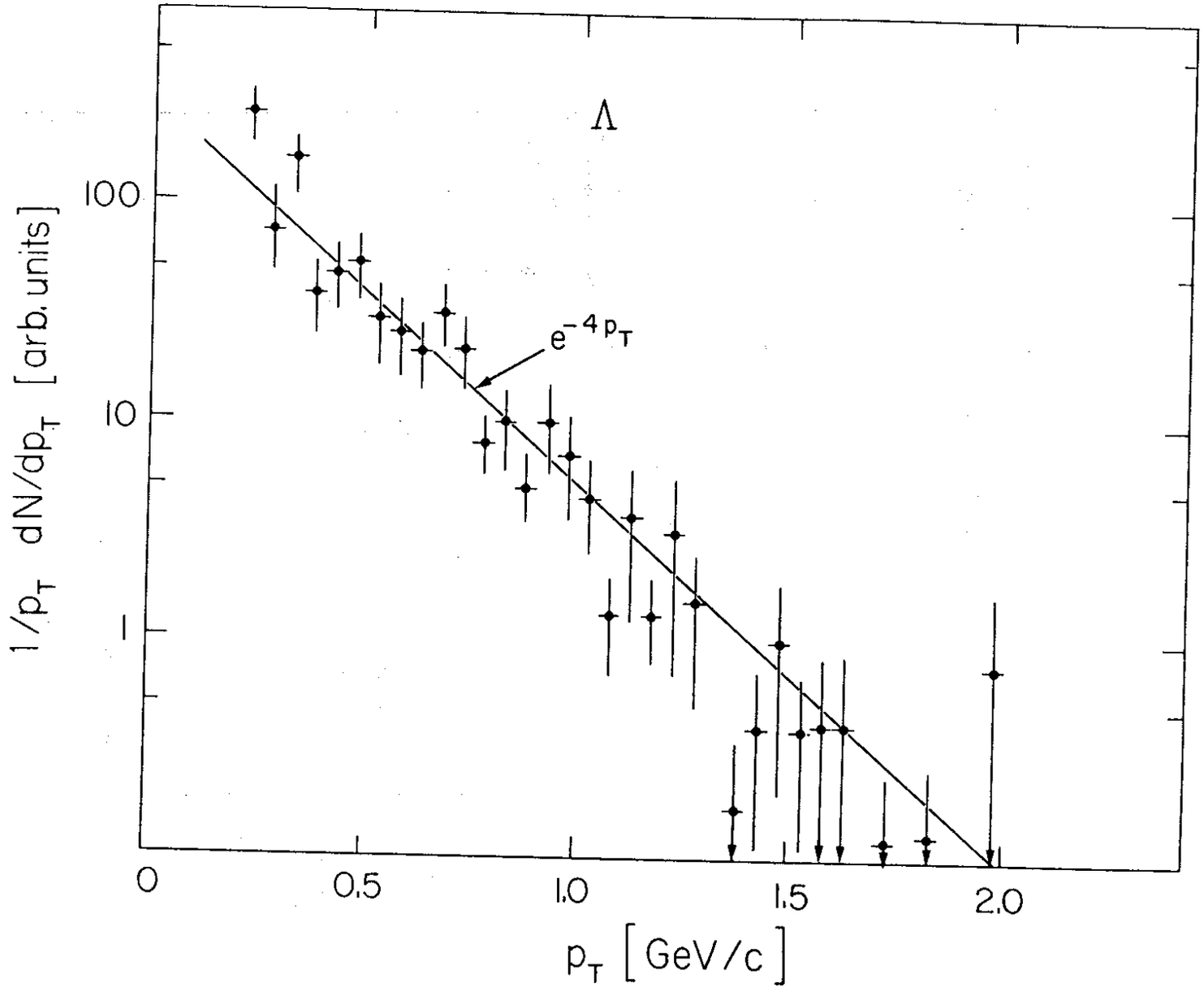

Fig. 13

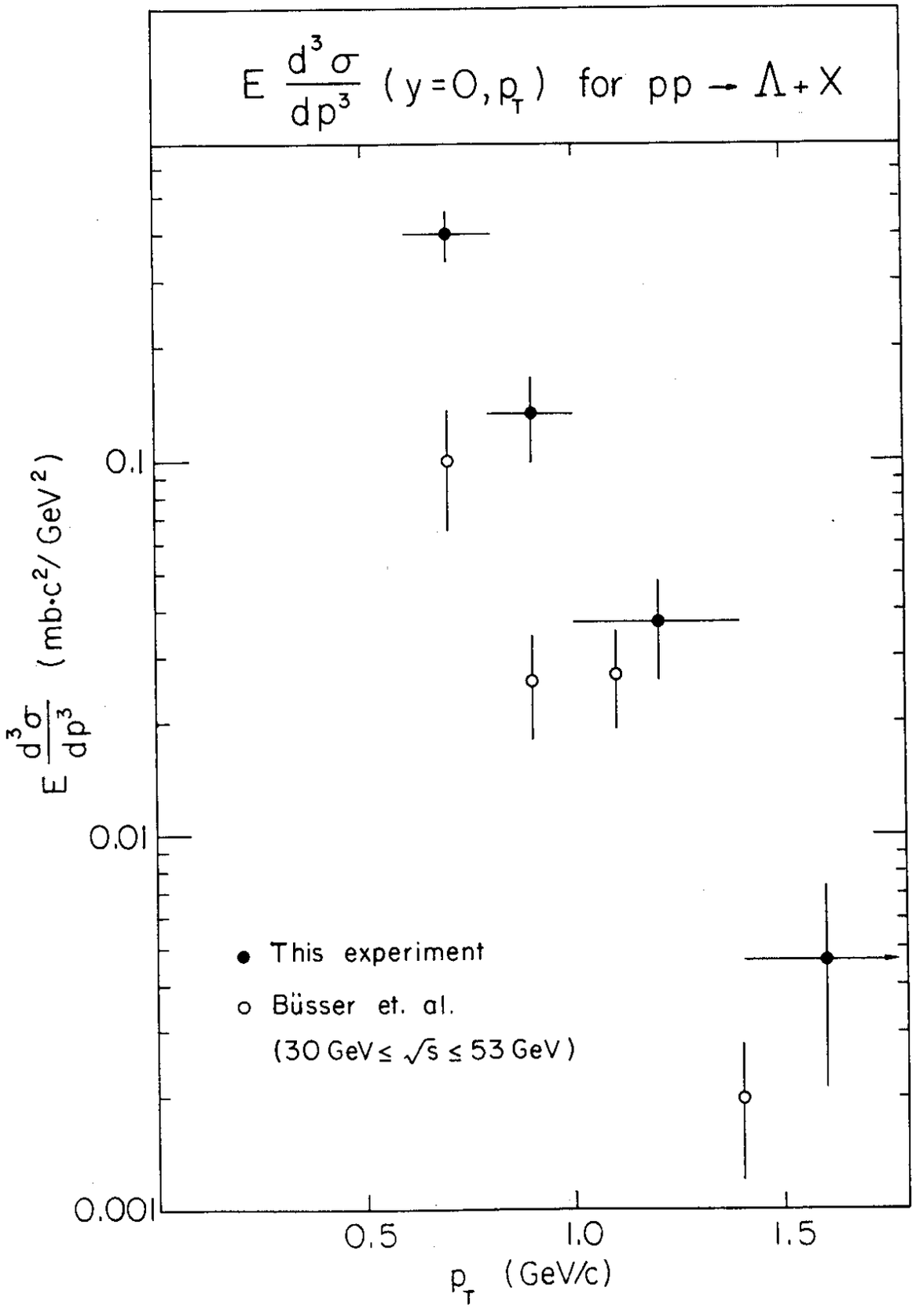
E d³σ/dp³ (y=0, p_T) for pp → Λ+X
E d³σ/dp³ (mb·c²/GeV²)
0.1
0.01
0.001
0.5
1.0
1.5
p_T (GeV/c)
● This experiment
○ Büsser et. al.
(30 GeV ≤ √s ≤ 53 GeV)

Fig. 14

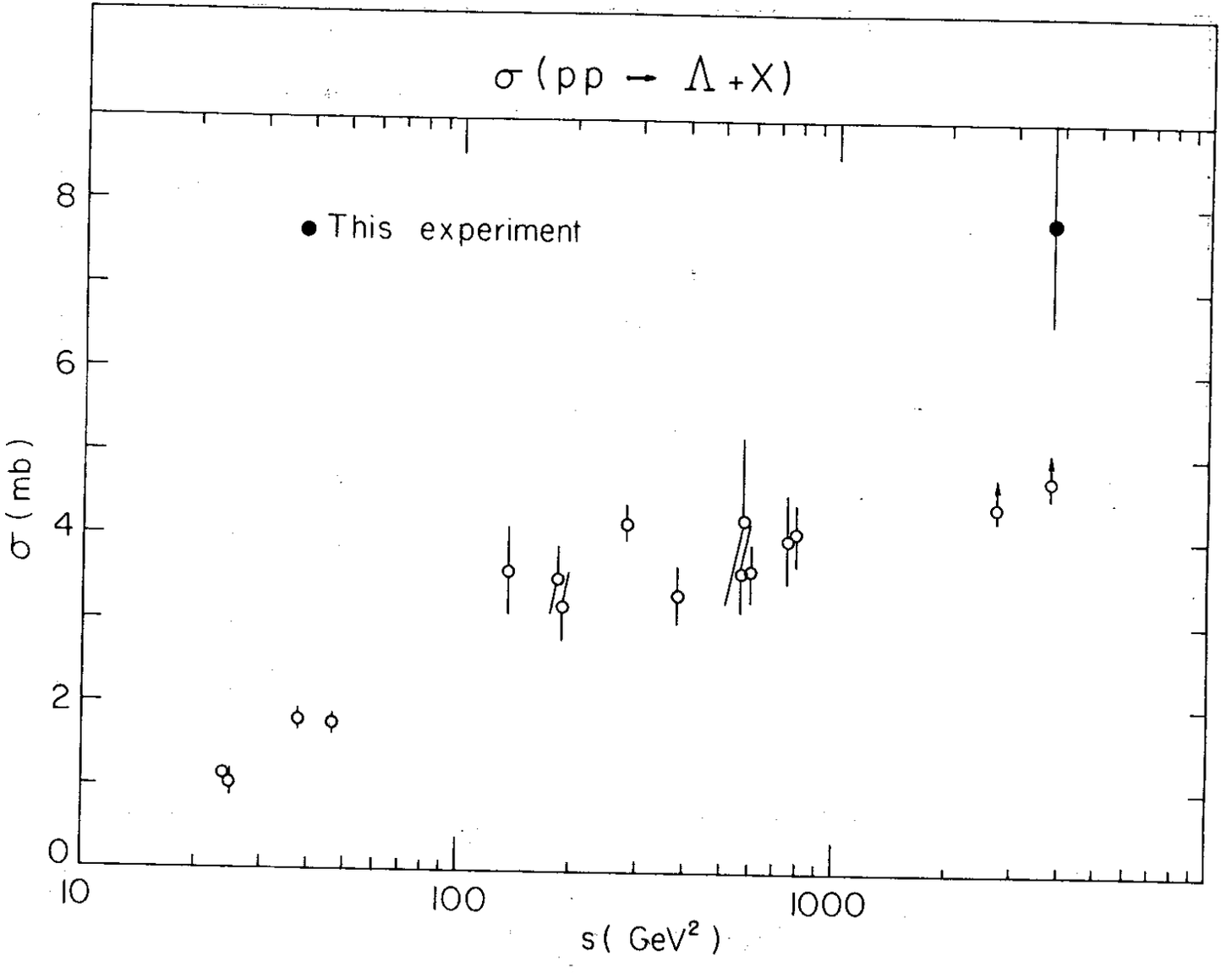

Fig. 15

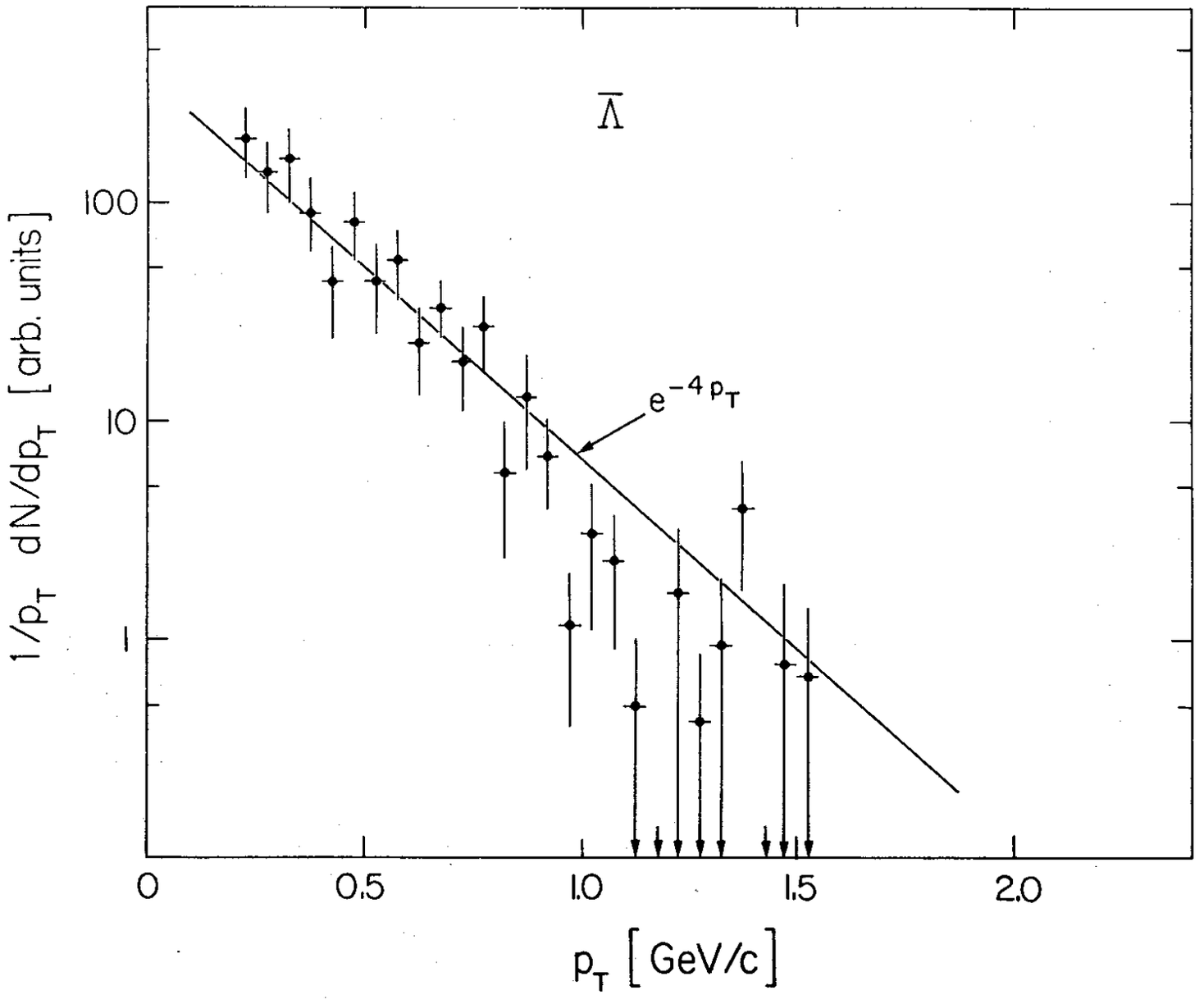
$\bar{\Lambda}$
100
10
1
$1/p_T \; dN/dp_T$ [arb. units]
$e^{-4\,p_T}$
0
0.5
1.0
1.5
2.0
p_T [GeV/c]

Fig. 16

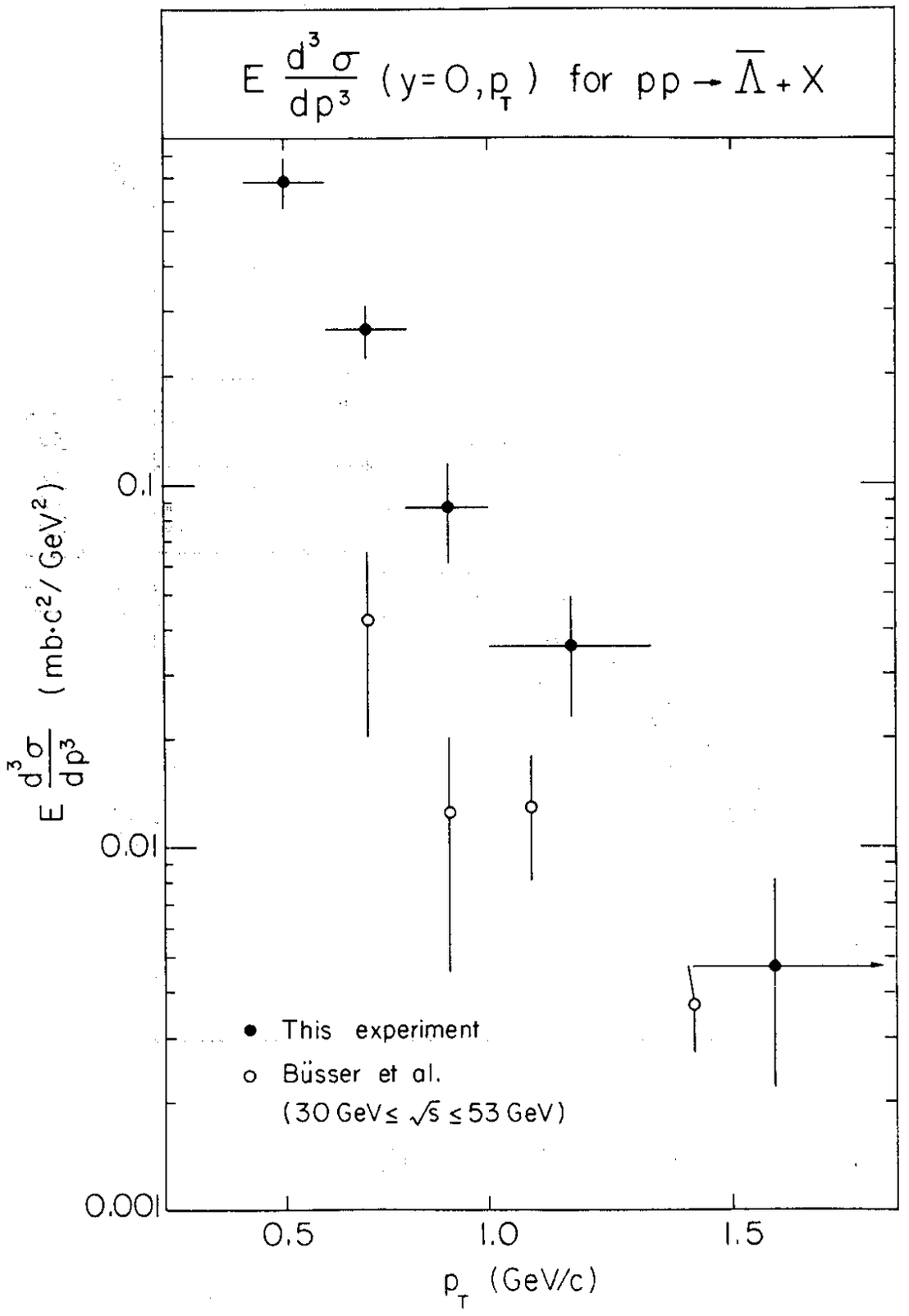
$E\frac{d^3\sigma}{dp^3}$ $(y=0, p_T)$ for $pp \to \bar{\Lambda} + X$
$E\frac{d^3\sigma}{dp^3}$ $(mb\cdot c^2/GeV^2)$
0.1
0.01
0.001
0.5
1.0
1.5
p_T (GeV/c)
● This experiment
○ Büsser et al.
(30 GeV ≤ $\sqrt{s}$ ≤ 53 GeV)

Fig. 17

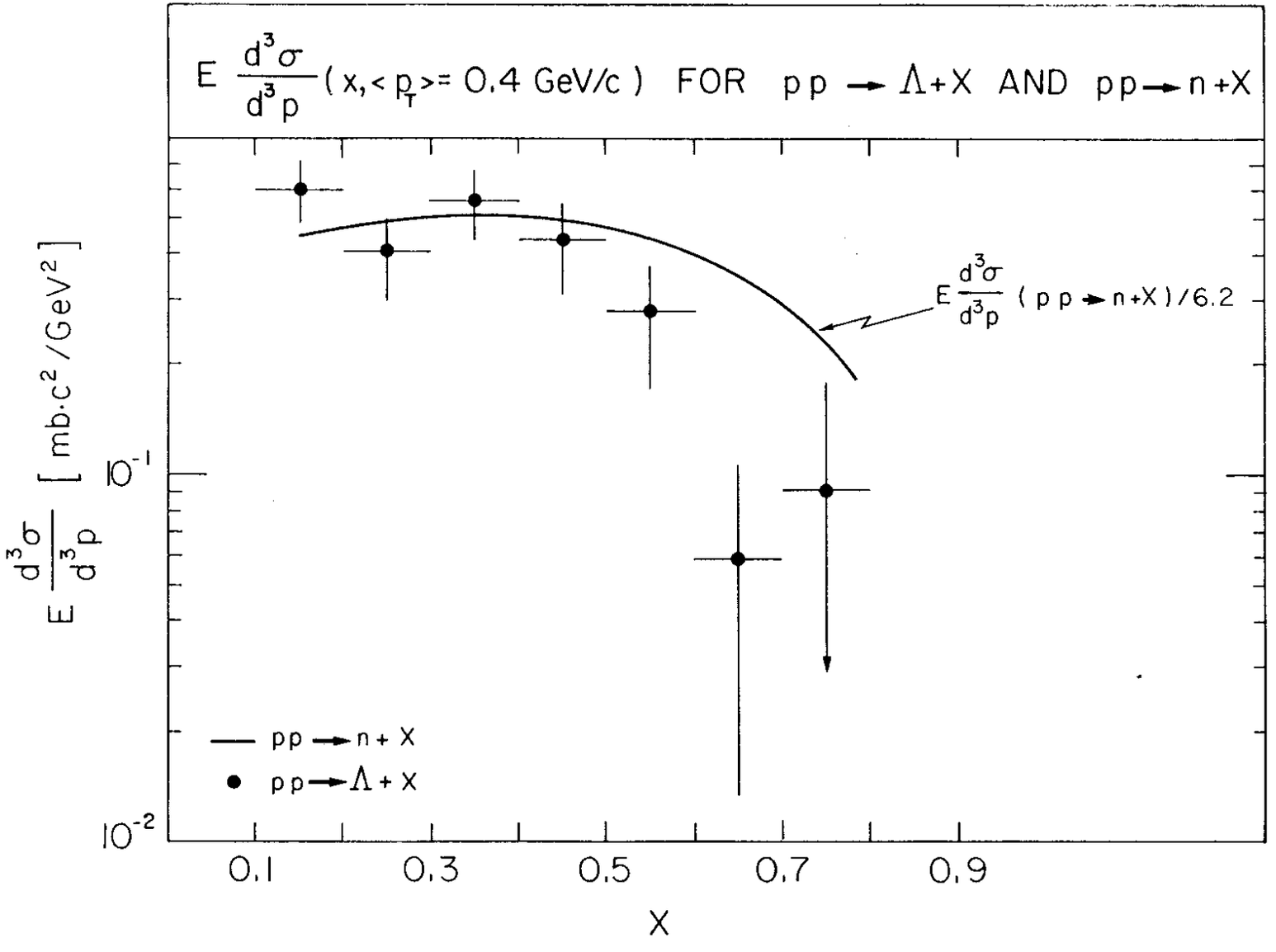
E d³σ/d³p (x, < p_T >= 0.4 GeV/c) FOR pp → Λ+X AND pp → n+X
E d³σ/d³p (pp → n+X)/6.2
E d³σ/d³p [mb·c²/GeV²]
10⁻¹
10⁻²
pp → n + X
pp → Λ + X
0.1
0.3
0.5
0.7
0.9
X

Fig. 18